BIOPHYSICS

A stretchable and strain-unperturbed pressure sensor for motion interference–free tactile monitoring on skins

Qi Su[1,2]†, Qiang Zou[2]†, Yang Li[1]†, Yuzhen Chen[3]†, Shan-Yuan Teng[4], Jane T. Kelleher[1], Romain Nith[4], Ping Cheng[1], Nan Li[1], Wei Liu[1], Shilei Dai[1], Youdi Liu[1], Alex Mazursky[4], Jie Xu[5], Lihua Jin[3], Pedro Lopes[4], Sihong Wang[1]*

A stretchable pressure sensor is a necessary tool for perceiving physical interactions that take place on soft/deformable skins present in human bodies, prosthetic limbs, or soft robots. However, all existing types of stretchable pressure sensors have an inherent limitation, which is the interference of stretching with pressure sensing accuracy. Here, we present a design for a highly stretchable and highly sensitive pressure sensor that can provide unaltered sensing performance under stretching, which is realized through the synergistic creations of an ionic capacitive sensing mechanism and a mechanically hierarchical microstructure. Via this optimized structure, our sensor exhibits 98% strain insensitivity up to 50% strain and a low pressure detection limit of 0.2 Pa. With the capability to provide all the desired characteristics for quantitative pressure sensing on a deformable surface, this sensor has been used to realize the accurate sensation of physical interactions on human or soft robotic skin.

INTRODUCTION

In any soft tissue, be it from a soft robotic or human skin, the pressure created through physical contacts on or inside the bodies not only acts as one of the major means to perceive tactile interactions but also carries physiological information regarding health conditions. Hence, soft pressure sensors that transduce mechanical stimuli into electrical signals are highly desirable to enable applications ranging from medical implants (*1*–*4*), wearable health monitoring (*5*–*10*), and prosthetic electronic (e)–skins (*11*, *12*) to technologies including soft robotics (*13*–*16*), human-machine interactions (*17*–*21*), and artificial intelligence (*22*, *23*). Since soft robots and human bodies generally perform movements with substantial deformations generated on their skins, tissues, and organs, it is indispensable to render such soft pressure sensors with comparable stretchability; in other words, we need pressure sensors that can function while conformably attached to surfaces under stretching deformation.

On the basis of the commonly used capacitive and piezoresistive sensing mechanisms, the past few years have witnessed the creation of stretchable pressure sensors, simply via using various types of stretchable conductors (*24*–*28*) and dielectric elastomers (*24*, *27*, *29*), which have already achieved high pressure sensitivity (*25*), large stretchability (*30*), and biodegradability (*31*). However, one key limitation remains, that is, the substantial alteration of quantitative pressure sensing performance when the sensor is under stretching, which arises from the inherent coupling of mechanical deformations along different directions of a structure. Hence, a longitudinal strain always causes normal compression, similar to the deformation from a normal pressure. This undesired sensing characteristic greatly complicates the application of such sensors for quantitative measurements of pressures under varied strain states. Although this problem could be mitigated at the system level by establishing a series of individually adjusted calibrations under different strains and having a real-time measurement of strain during the sensor's operation, this would only overcomplicate the sensing system by requiring precalibration and even recalibration in runtime while still sacrificing sensing fidelity.

So far, attempts for decoupling the strain's effect to the pressure sensing typically approach this by increasing the areal stiffness of individual pressure sensors on a stretchable substrate to isolate the sensor units from the applied strain (*24*, *27*). However, since the strain energy is dissipated only by the nonactive areas surrounding the sensors, this approach has three key limitations: (i) a challenge in achieving high sensing density in the case of sensor arrays, (ii) the enlarged dimension ratio of the nonactive areas under stretching, and (iii) the sacrificed skin/tissue conformability and biocompatibility of sensing areas with the increased stiffness. For the alternative avenue of enabling the intrinsic strain insensitivity from a sensor's design (*26*) and working mechanism, it remains highly challenging, and there have seen very few successes in achieving the desired performance.

Here, we report the design of a stretchable pressure sensor (Fig. 1A) that achieves intrinsically strain-unperturbed performance while providing a high pressure sensitivity of 4.5 and 2.0 kPa^{-1} in the pressure ranges of 0 to 1 and 1 to 10 kPa, respectively. This is realized through the synergistic creations of electrical double layer (EDL)–based interfacial capacitive sensing mechanism and the pyramid microstructure with designed stiffness hierarchy. Specifically, the use of an ionic elastomer for the micropyramids renders the sensor's overall capacitance dominated by the EDL formed at the interface between the tip of the pyramid and the top electrode (i.e., the C_{top} in the equivalent circuit in Fig. 1A), which remains almost unchanged (Fig. 1, B and D) under in-plane stretching. This is enabled by the patterned stiffening microelectrodes underneath each of the pyramids, together with the assist from a pair of soft spacers that keep the two ends of the sensor with the same separation distance between the top and bottom layers. Therefore, under

[1]Pritzker School of Molecular Engineering, The University of Chicago, Chicago, IL 60637, USA. [2]School of Microelectronics, Tianjin University, Tianjin, China. [3]Department of Mechanical and Aerospace Engineering, University of California, Los Angeles, Los Angeles, CA 90095, USA. [4]Department of Computer Science, The University of Chicago, Chicago, IL 60637, USA. [5]Nanotechnology and Science Division, Argonne National Laboratory, Lemont, IL 60439, USA.
*Corresponding author. Email: sihongwang@uchicago.edu
†These authors contributed equally to this work.

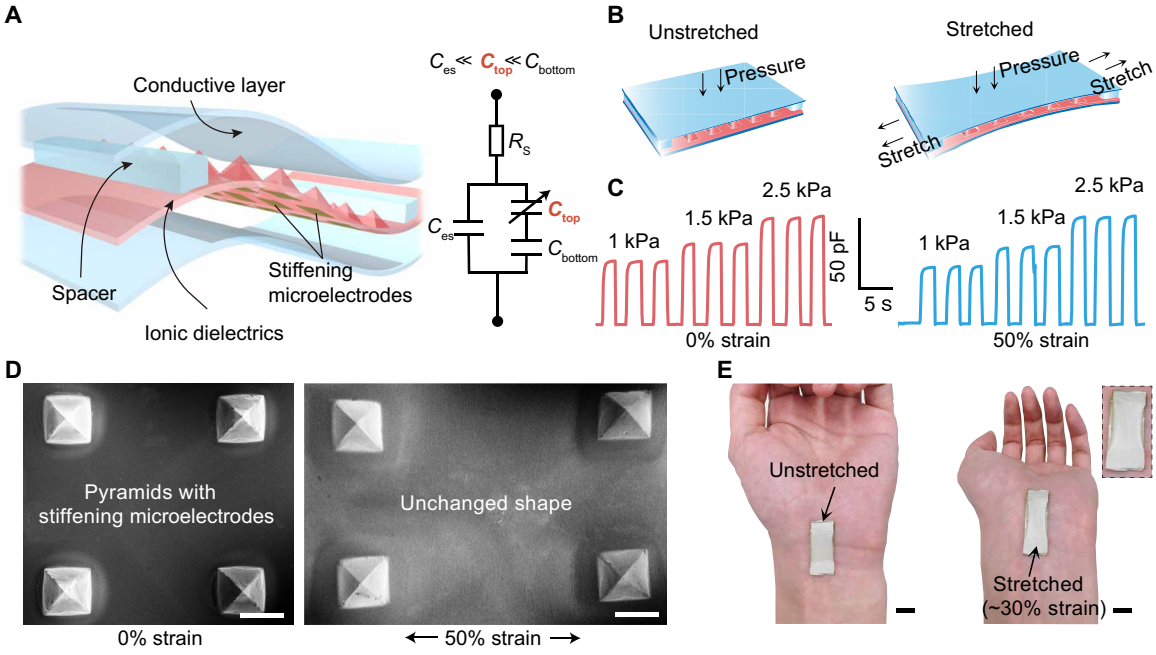

Fig. 1. Structure and strain-unperturbed performance of the stretchable pressure sensor. (**A**) Three-dimensional structure of the sensor and its equivalent circuit. C_{es} is the electrostatic capacitance between the top and bottom electrodes, and C_{top} and C_{bottom} are the electrical double layer (EDL) capacitances of the top interface and the bottom interface between the ionic dielectric and the electrode, respectively. The height of spacers is 350 μm, which is the same as that of the pyramids. (**B**) Schematic illustrations of the pressure sensor operating under unstretched (left) and stretched (right) states. (**C**) Capacitance responses as the sensing signal to three repeated pressure values when the sensor is unstretched (0% strain, left) and stretched (50% strain, right). (**D**) Scanning electron microscopy (SEM) images of the micropyramid structures with stiffening microelectrodes (at the backside) at 0 and 50% strains. Scale bars, 500 μm. (**E**) Photographs of the sensor attached to a hand wrist without and with outward bending. The inset picture is the enlarged view showing the maintained conformability of the sensor under skin deformation. Photo credit: S. Wang and Q. Su, The University of Chicago.

different strain states (Fig. 1B), the sensor can maintain not only a highly stable capacitance value when there is no pressure but also the same capacitance changing behaviors to normal pressures, as shown by the experimental data in Fig. 1C. Besides the strain-unperturbed performance, our design also provides a low detection limit and a high response speed to pressures as well as repeatable and robust sensing performance. The stretchability and low modulus of our sensor allow it to be attached to the human body or robots with soft embodiments and great conformability (Fig. 1E). Enabled by this unprecedented sensing capability, we have demonstrated its combination with a soft robotic hand for quantitative and closed-loop pressure control for remote medical palpation and therapy, as well as pressure sensing as a secondary e-skin.

RESULTS

Working mechanism and key components of the strain-unperturbed pressure sensor

When a normal pressure is applied to the sensor, the micropyramids will get compressed vertically, thus increasing the contact area between the pyramid tips and the top electrode (Fig. 2A, left). Therefore, the change of the capacitance value of the sensor, which is dominated by the EDL capacitance at this top interface, monotonically reflects the magnitude of the applied pressure. Compared to the commonly used electrostatic capacitance for pressure sensing, such EDL-type capacitance can provide much higher sensitivity. More uniquely, with this sensing mechanism, when the sensor is under an in-plane stretching, the capacitance value remains unchanged because our design maintains an unchanged contact area between the pyramids and the top electrode. To achieve this, the bases of the individual micropyramids are increased in stiffness by microscopically patterning a high-modulus material. Since the addition of this layer should not change the dominating role of the EDL at the top interface in the overall capacitance, this high-modulus material needs to be conductive so that such stiffening areas act as an extension of the bottom electrode. To satisfy these requirements with stiffening microelectrodes, a type of electrically conductive epoxy (MG Chemicals) is used. With this design, the strain applied to the sensor leaves pyramids' geometry virtually unaltered, which thus assists these pyramids in maintaining the same mechanical response to normal pressures (Fig. 2A, right). To further minimize the possible strain-induced squeezing between the top and bottom substrates, a pair of spacers with the same height as the pyramids is added at the two ends of the sensor. The unaltered pressure sensing performance is also confirmed by the finite-element simulations, in which the relations between the contact area and the pressure are identical at different strains, as shown in Fig. 2B (text S1 and fig. S1).

The fabrication process of the strain-unperturbed pressure sensor is shown in figs. S2 to S4. The pyramid structures are fabricated by molding on a premade Si template, and the stiffening microelectrodes are then blade coated on the bottom surfaces of the pyramids through a polyimide mask. The ionic elastomer, one of the key design elements in this sensor structure, is made by mixing a type of ionic liquid, 1-ethyl-3-methylimidazolium bis(trifluoromethylsulfonyl)imide

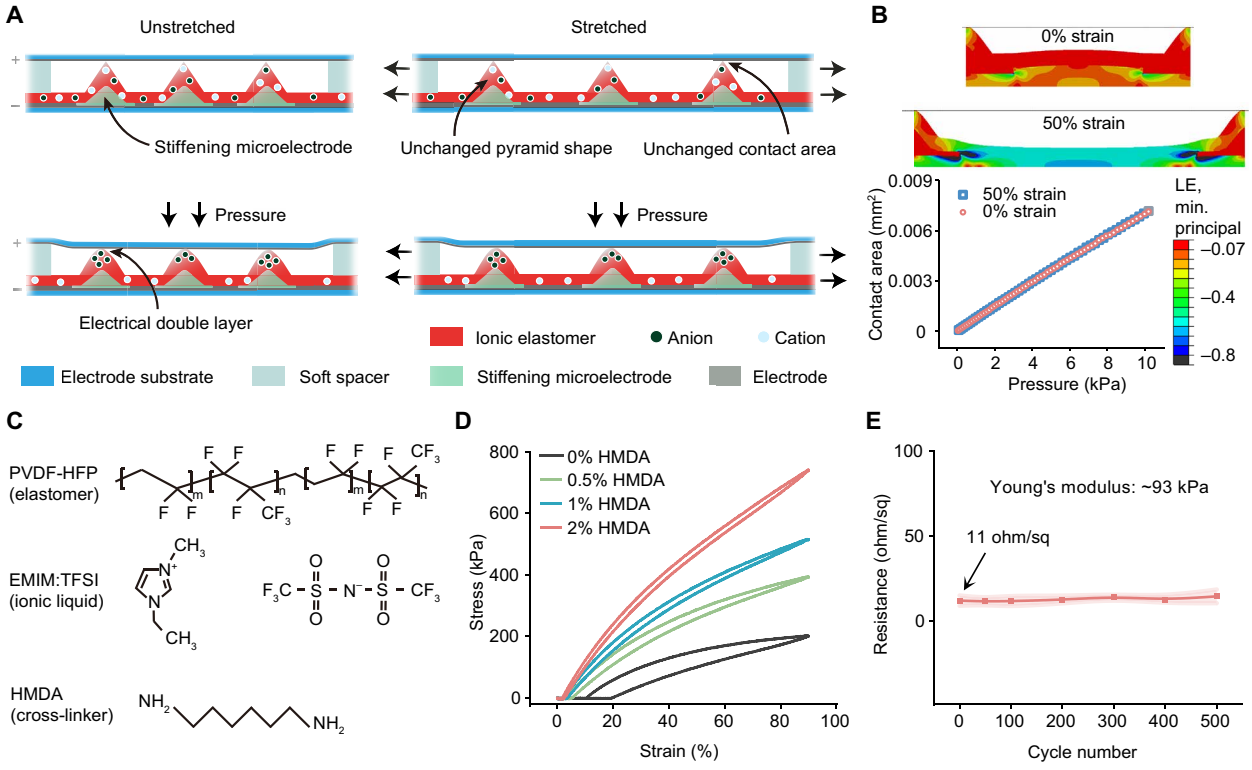

Fig. 2. Working mechanism and key components of the stretchable pressure sensor. (**A**) Schematic illustration of the pressure sensing mechanism that gives unaltered performances under stretching. (**B**) Finite-element simulation of the sensor's pressure sensing behavior. Top: The minimum principal logarithmic strain distribution in the dielectric layer under the normal pressure of 10 kPa when there are 0 and 50% in-plane strains. Bottom: Plot of the increase in the contact area between the pyramid tips and the top electrode surface under the increased pressure, which is proportional to the change of the EDL capacitance. Logarithmic strain (LE). (**C**) Chemical structures of the three components used in the ionic elastomer: PVDF-HFP (elastomer, top), EMIM:TFSI (ionic liquid, middle), and HMDA (cross-linker, bottom). (**D**) Cyclic stress-strain curves of four ionic elastomer films all containing 30 wt % of EMIM:TFSI but different percentages of HMDA. (**E**) Evolvement of the sheet resistance of the stretchable Ag nanoparticle electrode during 500 cycles of repeated stretching to 50% strain. Error bar was calculated with five electrodes.

(EMIM:TFSI), into the matrix of poly(vinylidene fluoride-co-hexafluoropropylene) (PVDF-HFP) (Fig. 2C), which is an elastomer with a relatively high dielectric constant of 9 to facilitate ion delocalization (*32*). When such an ionic elastomer is fabricated into capacitors, it is found that a higher amount of the ionic liquid blended into the elastomer provides a higher capacitance, which is a favorable condition for achieving a higher sensitivity (fig. S5). However, this is accompanied by an increase in viscoelastic behavior (fig. S6), which will prevent such a layer from reverting to its original dimension. Therefore, a moderate weight percentage of 30% is chosen for the ionic liquid. To restore the desired elasticity for reversible deformation, we crosslink the film by adding hexamethylenediamine (HMDA) as the cross-linker (Fig. 2, C and D, fig. S7, and text S2) (*33*). A cyclic stretching testing shows that the increased amount of HMDA helps both the suppression of viscoelastic behavior and the increase in Young's modulus. When its amount is equal to or above 1 weight (wt) %, the film can fully return to its original length after stretching (fig. S8). However, since we found that the crosslinking causes EDL capacitance to decrease (fig. S9), we therefore opted to use 1 wt % for HMDA. For another main functional element in the sensor, the stretchable electrodes, we used a type of stretchable Ag nanoparticle paste, which is blade coated on a piece of Ecoflex substrate to achieve a low modulus (fig. S10). When acting as the top electrode, this low modulus can ensure that the applied pressure can be effectively transduced to the compression of the pyramids, which is also important for the strain-unperturbed performance. Because of the good stretchability of this Ag paste and its strong adhesion to Ecoflex, the electrode is highly stretchable (fig. S11), with minimal increase in the resistance during 500 cycles of repeated stretching to 50% strain (Fig. 2E).

Validation of the strain-unperturbed pressure sensing from the designed structure

Since the pressure sensor can be stretched to at least 50% strain before the ionic dielectric layer starts to delaminate from the bottom electrode, the sensor's performance is systematically characterized under the stretching states of 0, 25, and 50% strains, each with a pressure range of 0 to 10 kPa (Fig. 3A and fig. S12). The resulting signal is the sensor's capacitance, measured at 1 kHz. As shown in Fig. 3A, the pressure sensing behaviors from four pieces of separately fabricated sensors show good linearity over two continuous pressure ranges, with virtually identical performance, and high sensitivity of 4.5 kPa^{-1} in 0 to 1 kPa and 2.0 kPa^{-1} in 1 to 10 kPa, respectively. When these pressure sensors are stretched from 0 to 50% strain, almost no change in performance is observed (Fig. 3A, fig. S12, and movie S1). From a more quantitative analysis, the capacitance readings for different pressures applied with no strain and then with 50% strain vary by only about 2% on average; this can be regarded

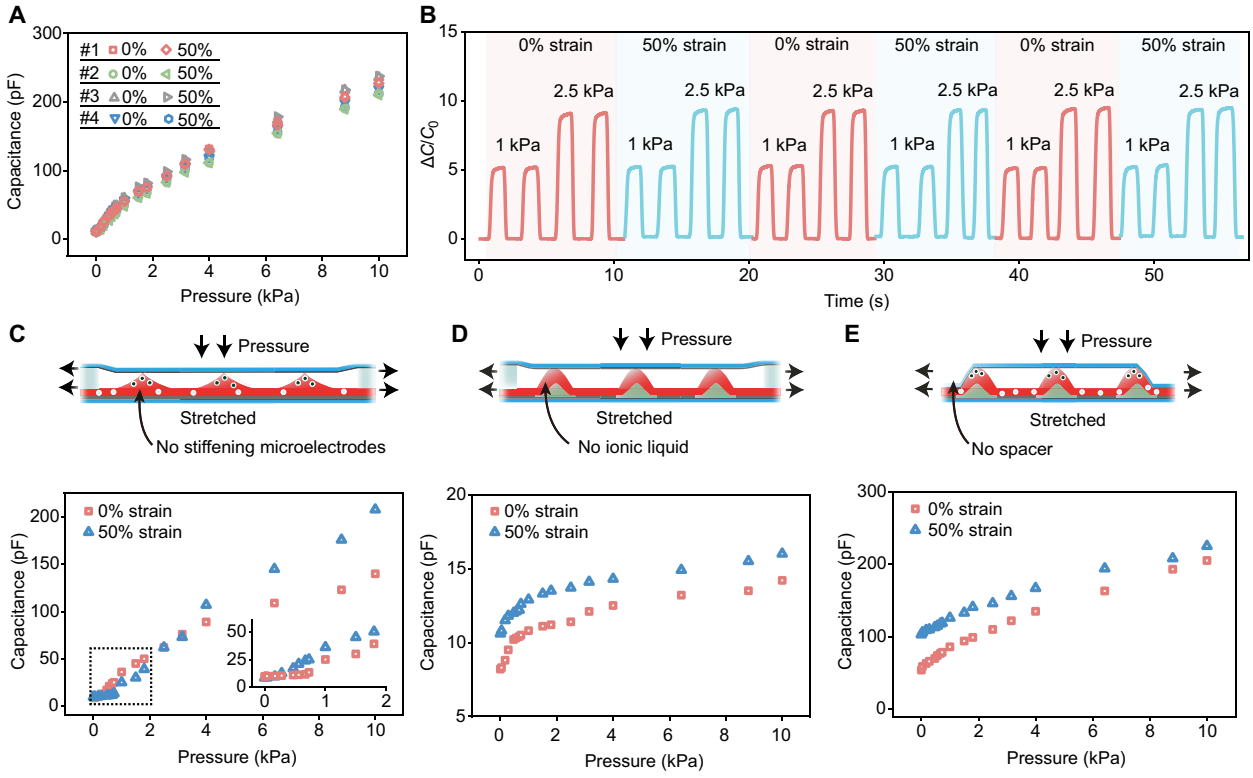

Fig. 3. Characterization of the stretchable pressure sensor's performance and experimental validation of the mechanism for the strain-unperturbed behavior. (**A**) Capacitance responses to pressures from four separately fabricated sensors when they are at 0 and 50% strains. (**B**) Typical performance repeatability of the sensor under repeated pressure loading and repeated stretching cycles between 0 and 50% strains. C_0 is the initial capacitance, and ΔC is the capacitance change. (**C** to **E**) Pressure sensing performances under stretching from the reference sensors without stiffening microelectrodes (C), without ionic effect in the elastomer layer (D), and without soft spacers (E), respectively.

as a strain insensitivity of 98%. Besides uniaxial stretching, our sensor also presents strain-unperturbed pressure sensing performance in biaxial stretching (fig. S13). Moreover, this strain-unperturbed pressure sensing performance is well maintained during repeated stretching cycles to 50% strain (Fig. 3B). Through finite-element simulations and experimental results, we also confirm that the strain-unperturbed pressure sensing can be obtained with varied pyramid densities (fig. S14 and text S3) and ionic elastomer thicknesses (fig. S15). Thus, pyramid density and thickness are the structural variables by which the sensitivity and the sensing range can be tuned to meet the requirements of different applications. Even under varied levels of humidity and/or temperature, the sensor can maintain the strain-unperturbed sensing performance (fig. S16).

To further experimentally validate the roles of the key design features, i.e., the stiffening microelectrodes, the EDL capacitance from the ionic elastomer, and the soft spacers, we fabricated and characterized several types of reference sensors, each without one of these features. First, when we do not include the stiffening microelectrodes, the stretching nonnegligibly alters the pressure sensing performance over the entire pressure sensing range. The capacitance readings taken under the same pressure with no stretching and at 50% strain can change by as much as 50%. This is simply due to the flattening of the pyramids under the in-plane stretching (fig. S17), which causes the contact area with the top electrode to increase. Second, we fabricate a sensor with the pyramids made from a nonionic elastomer (i.e., PVDF-HFP), therefore turning the sensor into an electrostatic capacitor. Besides the expected decrease in the capacitance values and sensitivity, the pressure sensing performance also shifted under stretching (Fig. 3D and fig. S18). Although the stiffened pyramid structures are not subject to the stretching, there is still a slight decrease in the distance between the top and bottom electrodes in the areas between the pyramids, as well as an increase in the overlapped area between the top and bottom electrode, which overall serve to determine the electrostatic capacitance. Last, when the spacers are not included in the design of our sensor (Fig. 3E), the strain-unperturbed pressure sensing performance cannot be achieved because of the nonideal contact between the pyramids and the top electrode at the two ends of the sensors. In addition, reference sensors (text S4) were also made to show the indispensable roles of the adhesive layer between the pyramid structures and the bottom electrode (fig. S19) as well as the low thickness (fig. S20) and the low stiffness (fig. S21) of the top substrate.

Comprehensive characterization of the sensor's performance

Next, we proceed to characterize the other main performance characteristics of our sensor, including its pressure detection limit, its stability, and its response time. Through testing the sensor performance under ultralow pressure, its detection limit can be as small as ca. 0.2 Pa (Fig. 4A), which is the pressure created by a small piece of

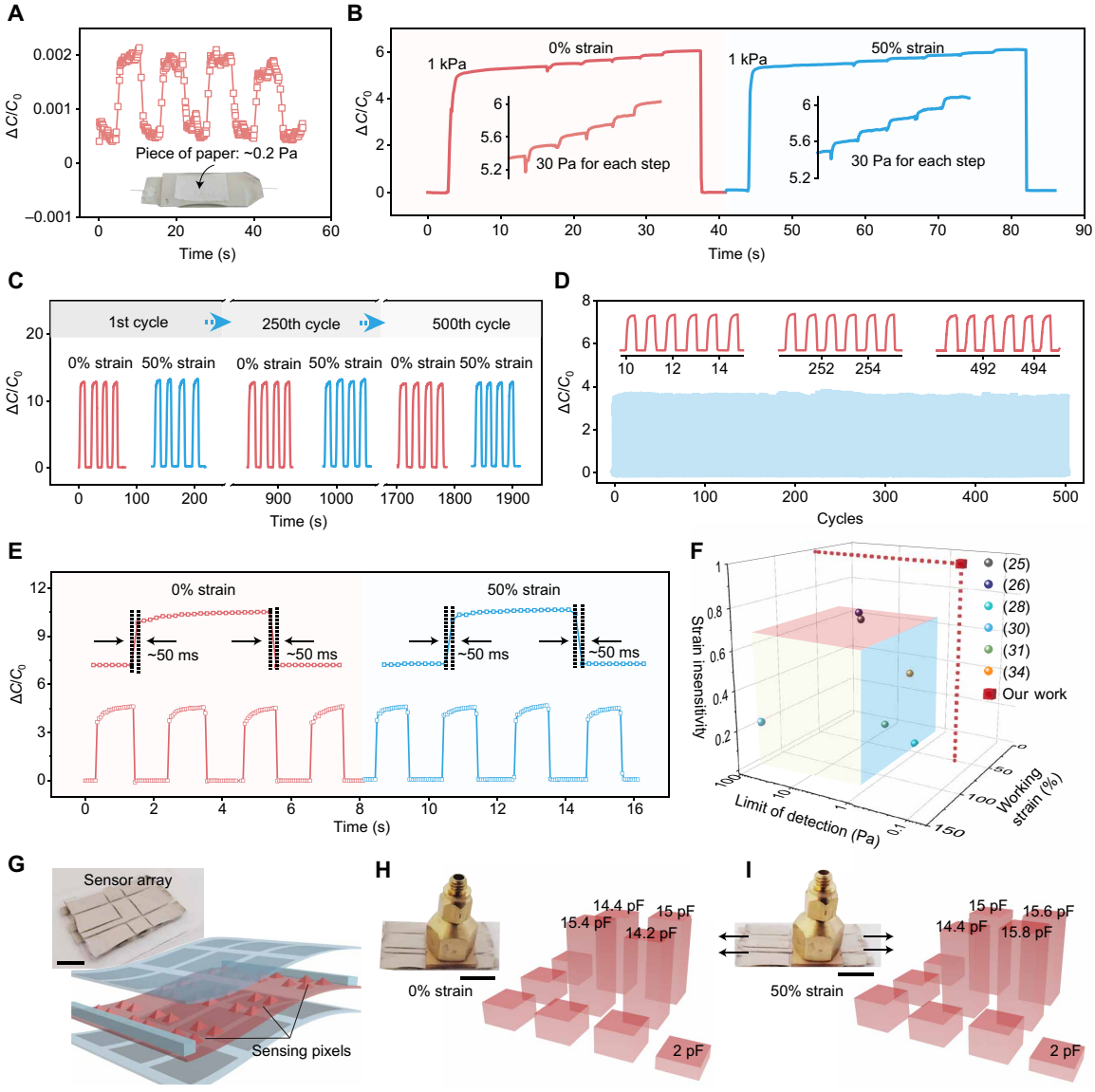

Fig. 4. Response characteristics of the stretchable pressure sensor. (**A**) Capacitance response of the sensor under a pressure at the level of its limit of detection (i.e., 0.2 Pa), which is created by a small piece of paper placed on the sensor (inset). (**B**) This sensor's capability of recognizing small changes of pressure (e.g., by 30 Pa) on top of a large pressure (e.g., 1 kPa) when it is at both 0 and 50% strains. (**C** and **D**) Fatigue tests of the sensor with 500 cycles of repeated stretching to 50% strain and pressure loading of 4 kPa (C) and with 500 cycles of repeated pressure loading of 0.67 kPa under 0% strain (D). (**E**) Response speed of the sensor at both 0 (left) and 50% strains (right). (**F**) Comparison of our sensor with previously reported stretchable pressure sensors in three key performance parameters: limit of detection (preferred to be lower), maximum working strain (preferred to be higher), and strain insensitivity (needs to approach 1). (**G**) Three-dimensional structure and the photograph (inset) of the sensor array. Scale bar, 10 mm. (**H** and **I**) Pressure distribution mapping by the sensor array at 0 (H) and 50% (I) strain. Scale bars, 10 mm. Photo credit: S. Wang and Q. Su, The University of Chicago.

paper placed on the sensor. In addition, even when the sensor is operating under a relatively high pressure (e.g., 1 kPa), it still has very good recognition to small changes of pressure (e.g., by 30 Pa, as shown in Fig. 4B) on top, under both strain-free and stretched conditions, which reflect the accuracy and steadiness of the sensing performance. To test the stability of the performance of our sensor, we applied repeated stretching to 50% strain for 500 cycles (Fig. 4C) and repeated pressure loading with 0.67 kPa for 500 cycles under 0 and 50% strain (Fig. 4D and fig. S22). In both cases, no changes in either the pressure sensing performance or the strain-unperturbed characteristics were observed. Moreover, the dynamic sensing performance has a short response time of ~50 ms to both the loading and unloading of pressure (Fig. 4E), which is not affected by stretching either. When compared with all the reported stretchable pressure sensors in published works, our sensor is the only one to attain all the three key performance characteristics simultaneously: low detection limit (i.e., high sensitivity) for pressure, high stretchability, and strain-insensitive performance (Fig. 4F and table S1) (*25*, *26*, *28*, *30*, *31*, *34*). Our design for strain-unperturbed pressure sensing can be further integrated into a sensor array (Fig. 4G and

fig. S23), which can provide pixelated, highly quantitative, and strain-unperturbed measurement under large stretching up to 50% strain (Fig. 4, H and I).

Proof-of-concept demonstrations

The stretchability and strain-unperturbed performance of our sensor allow us to quantitatively measure pressures at soft and deformable surfaces, such as human tissue/skin or soft robots. We demonstrate, at the example of two distinct applications (Fig. 5), how to leverage our pressure sensor to enables precise measurement and control of pressures (i) to digitally record touch information on human limbs, which deform as they have motions, and (ii) to quantitatively sensorize a pneumatically actuated soft hand of a medical soft robot, allowing it to precisely calibrate their force feedback controller to regulate the pressure apply onto or record physiological pressures (e.g., pulse) from patients' bodies.

Our first representative application demonstrates our stretchable pressure sensor as a secondary e-skin either on a human skin to digitally record touch information for the neurological understanding of mechanical sensation process or on prosthetic limbs to accurately restore the touch sensation without being influenced by limb's movements. To demonstrate this, a sensor with a responsive area of 3×3 mm^2 is attached to the skin to measure various types of touch such as the user's wrist bends. As shown in Fig. 5 (A to C), the high sensitivity of the sensor enables quantitative recognition of different types of touches, including finger touch, palm pressing, and contact with another soft object, with varied lightness and durations (movies S2 to S4). There is minimal change of capacitance signals resulting from the wrist bending under the same type of touch, which is afforded by the strain-unperturbed performance of this sensor.

Our second representative application is on soft robots for patient/elderly care, physical diagnosis, and therapy, which hinges on the precise control of the force applied in interactions between a robot and a patient's body. Through accurately measuring the pressure in real time between the end effector of a robotic soft hand and a human body during palpation or therapy and sending the information to a remote system operated by a doctor, the doctor can then perform remote diagnosis and/or therapy through controlling the robotic hand to exert well-controlled pressures onto a patient's body (Fig. 5D). To demonstrate this, we attached a stretchable pressure sensor to the fingertip of a pneumatically actuated soft robotic hand that is connected to a motorized robotic arm for executing its movement (Fig. 5E). In this way, the soft robotic hand can be moved by the robotic arm to make contact for, applying, and/or measuring dynamic pressure to/from another object such as a human body in the scenario of physical therapy and palpation. To realize the programmed control of the pressure applied by the soft robotic hand, which is a core function needed in physical therapy, the stretchable pressure sensor (Fig. 5F) can serve to provide real-time pressure values, which is fed to the closed-loop controller of the robotic arm, for achieving preset pressure values (figs. S24 and S25 and movies S5 and S6). We first demonstrate the unperturbed pressure sensing and control capability by having the soft robotic finger press onto a human arm, during which the robotic finger can be pneumatically actuated to bend, thereby causing stretching to the pressure sensor. As shown in Fig. 5G and movie S7, the signal from the pressure sensor remained very stable during the bending of the finger for making a good contact to a side location of the arm and only started to sharply change when the finger got in touch with the arm. With the continuous monitoring of the pressure, the robotic hand can self-adjust its position to reach and maintain the preset pressure, even when there is a movement of the arm. The strain-unperturbed property ensures the altered sensing accuracy compared to the undeformed robotic finger (fig. S26 and movie S8). For the use on remote diagnosis, such sensorized soft robotic finger can serve to form good contact and measure mechanical physiological signals, e.g., arterial pulse, from the skin. As shown in Fig. 5H, fig. S27, and movies S9 and S10, when the robotic fingertip bends and touches the side of a wrist, highly accurate and motion-unperturbed recording of the pulse train can be achieved. This shows the future perspective for enabling robotic medical diagnosis by our stretchable and strain-unperturbed pressure sensor.

DISCUSSION

By creating a design strategy that synergistically combines the interfacial-capacitive pressure sensing mechanism and the mechanically hierarchical micropyramid arrays, we presented a stretchable pressure sensor that unprecedentedly realized strain/motion-unperturbed and highly accurate tactile monitoring on a soft and stretching surface, such as a soft robotic or human skin. In particular, this sensor provides a suite of critically important performance characteristics, including high sensitivity to pressure, high stretchability, unaltered pressure sensing performance under stretching, good linearity over a wide pressure range, fast response speed, highly repeatable, and robust performance. Enabled by these properties, collectively, our strain-unperturbed stretchable pressure sensor can fill in the open need of quantitatively sensorizing and/or digitizing the tactile sensation on human and robotic skins, which is demonstrated by quantitatively measuring the touch sensation on a deforming human skin and also by the combination with a soft robotic system for realizing remote physical palpation and therapy. Other highly valuable application areas include, but are not limited to, rehabilitation and prosthesis for body joint areas that have large body deformations.

MATERIALS AND METHODS

Materials

Stretchable Ag nanoparticle paste 126-49 was purchased from Creative Materials. Tetramethylammonium hydroxide (TMAH) solution (25 wt % in H_2O) and HMDA were purchased from Sigma-Aldrich and used as received. EMIM:TFSI was purchased from TCI America and used as received. Both silicone adhesive and Ecoflex 00-10 were purchased from Smooth-On. Electrically conductive epoxy adhesive 8331 was purchased from MG Chemicals. PVDF-HFP FC2299 was supplied by 3M Dyneon Fluoroelastomer and used as received. Polydimethylsiloxane (PDMS) Sylgard 184 was purchased from Dow Corning.

Fabrication of the strain-unperturbed pressure sensor

PVDF-HFP was dissolved in acetone with a weight ratio of 1:6. The ionic liquid EMIM:TFSI was added into the mixture in varied amounts with weight ratios of 15, 30, and 60%. The solution was stirred at room temperature for ~4 hours. HMDA was dissolved in acetone with a concentration of 80 mg/ml and added into PVDF-HFP/EMIM:TFSI solution and stirred at 300 revolutions per minute (rpm) for 10 min.

To create a silicon mold, a layer of photoresist (AZ 703) was spin coated on a Si/SiO_2 wafer. After baking and exposure, the Si/SiO_2 wafer was patterned by reactive ion etching to produce a square

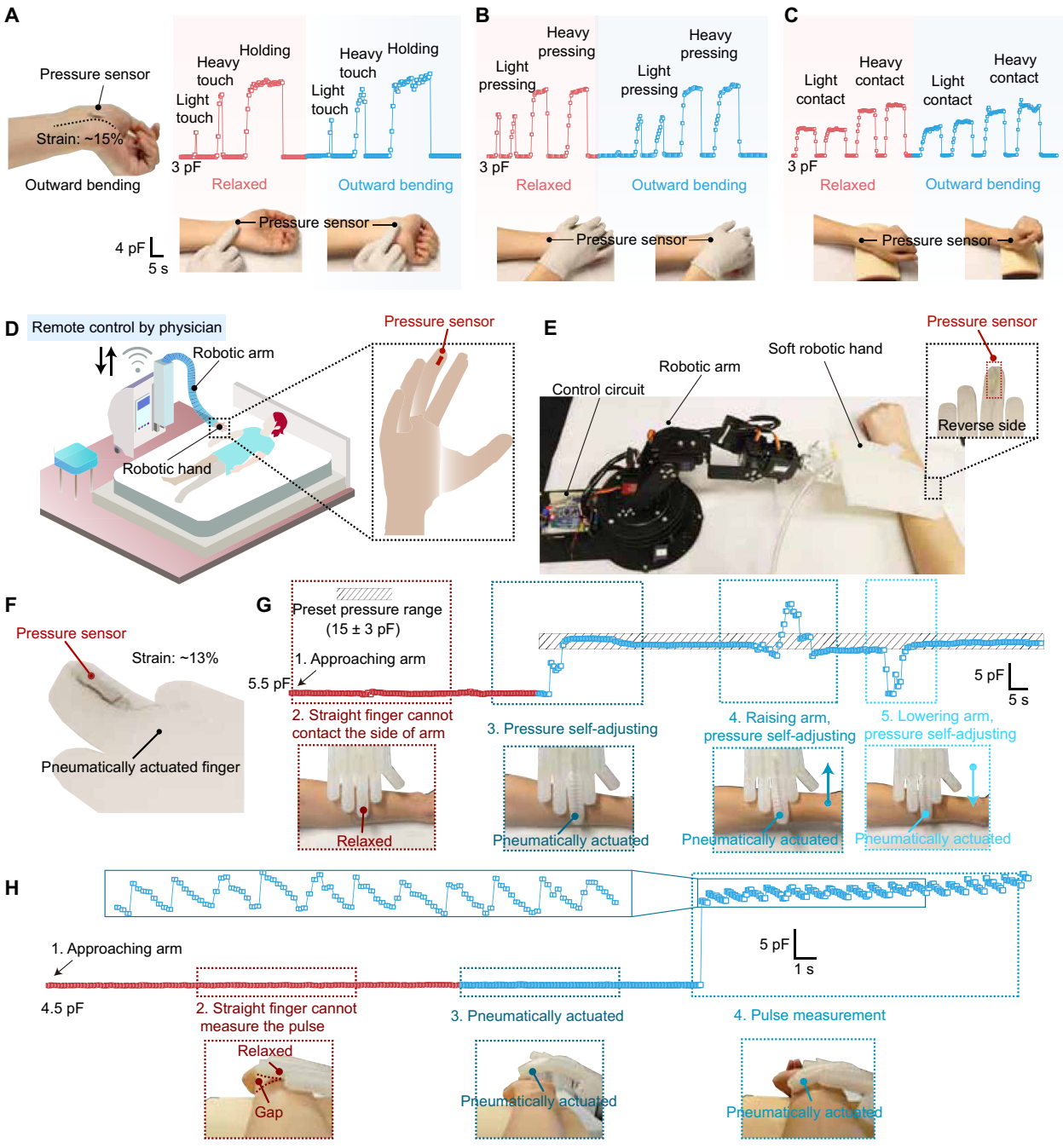

Fig. 5. Use of the stretchable pressure sensor for second e-skin and soft robotic applications. (**A** to **C**) The sensor serving as a secondary e-skin on a human (or prosthetic) wrist for providing quantitative sensation to various types of touches: finger touch (A), hand palm touch (B), and touch with a soft object (C) when the wrist is in both the relaxed and outward bending (strain: ~15%) positions. (**D**) Schematic scenario of using the stretchable pressure sensor on a pneumatically actuasoft robotic hand to realize remote physical diagnosis and therapy on patients. (**E**) Picture of the experimental setup for demonstrating a sensorized robotic fingertip on the soft hand controlled by a robotic arm to touch, apply, and measure pressure to/from a human arm. (**F**) Picture of the pressure sensor attached on the pneumatically actuated robotic finger with a strain of ~13%. (**G**) Real-time capacitance reading from the pressure sensor integrated on a soft robotic fingertip, which enables the closed-loop control of its attached robotic arm for applying and self-adjusting a force, with a preset pressure value, onto the top surface of a human arm. (**H**) The process recorded for the robotic finger applying and self-adjusting a force to the wrist to measure arterial pulse signals, during which the robotic finger needs to bend through the pneumatic actuation (i.e., stretching) to have a conformal contact with the skin. Photo credit: S. Wang and Q. Su, The University of Chicago.

array of opened windows (500 × 500 μm^2) with exposed Si. Next, an inverted pyramid array with a height of 350 μm was developed by wet etching with TMAH solution (5 wt % in H_2O) at 80°C.

Then, the surface of the Si mold was modified by O_2 plasma (400 W, 200 mtorr) to enhance its hydrophilicity. A sacrificial layer of dextran (5 wt % in water) was spin coated on the Si mold at 3000 rpm for 30 s, followed by annealing at 80°C for 10 min. PVDF-HFP/EMIM:TFSI/HMDA ionic elastomer was drop casted onto the Si mold and then cured at room temperature for 4 hours to form a dielectric layer of 160 μm. Subsequently, a polyimide mask was placed atop the dielectric layer so that its pattern aligned with the pyramids. An electrically conductive epoxy adhesive was blade coated across the masked dielectric layer and on the bottom surface of the pyramids; the mask was removed, leaving a stiffening pixel on the base of each pyramid. After curing the stiffening microelectrodes at 80°C for 10 min, the sacrificial layer was dissolved, and the dielectric layer was peeled off from the Si mold. PDMS film with a thickness of 350 μm was cut into the required dimension (14 × 4 × 0.35 mm^3) for the two spacers and then bonded to the two short edges of the dielectric layer, 2 mm away from the pyramid microstructure.

To construct the bottom and top electrode substrates, Si/SiO_2 wafers with dextran sacrificial layers were coated with Ecoflex 00-10 (part A:part B = 1:1) by spin coating at 1500 rpm for 30 s and at 3500 rpm for 30s, respectively. Next, a patterned polyimide mask was affixed to the elastomer-coated wafer, and an Ag nanoparticle paste layer (~50 μm) was added by blade coating, followed by curing at 150°C for 30 min. Then, the electrode was peeled off from the Si wafer by dissolving the sacrificial layer; the top electrode was completed at this point. For the bottom electrode only, another Ag nanoparticle paste layer, which would act as the adhesive layer, was added by blade coating. After this, the dielectric layer with two spacers was placed on top of the adhesive layer to assemble the lower part (this includes the bottom electrode, adhesive layer, and dielectric layer) of the sensor. The lower part of the sensor was precured at 80°C for 1 hour and then post cured at 150°C for 5 min. Last, the top electrode was bonded to the two spacers to complete the sensor.

Fabrication of sensor array

First, the solution of ionic elastomer was drop casted on a silicon mold, with the pyramidal pattern designed for a sensor array (3 × 3 U, 9 mm^2 for each unit), and cured to form an ionic microstructured dielectric layer. Then, the electrically conductive epoxy adhesive was blade coated onto each base of pyramids, with the patterned mask as stiffening microelectrodes. Before the dielectric layer was peeled off from the silicon mold, the stiffening microelectrodes were cured at 80°C. Top and bottom electrodes were prepared by blade coating stretchable Ag nanoparticle paste onto stretchable substrates of Ecoflex 00-10. Next, the ionic dielectric layer was bonded to the bottom electrode with a layer of the stretchable Ag nanoparticle paste in between, which was then cured to act as an adhesive layer. Last, two soft spacers were bonded to the two edges of the dielectric layer, and then the top electrode was bonded to the two soft spacers to form a sensor array.

Fabrication of reference sensors

For the fabrication of reference sensors, all steps and parameters are consistent with those of our sensor, except the experimental variables. To fabricate a reference sensor without stiffening microelectrodes, the dielectric layer was directly peeled off of the Si mold after curing, without blade coating the stiffening microelectrodes of electrically conductive epoxy adhesive. For a reference sensor without ionic liquid (0 wt %), no ionic liquid was added into PVDF-HFP/HMDA solution. The reference sensor without spacers was fabricated by bonding two terminals of the top electrode directly to the edge of the pyramid structure. The adhesive layer was not blade coated on the bottom electrode before assembling the dielectric layer to fabricate a reference sensor without the adhesive layer. PDMS substrate film and Ecoflex substrate films with different thicknesses were used to build reference sensors.

Ionic elastomer and electrode characterizations

To characterize the mechanical performance of PVDF-HFP/EMIM:TFSI/HMDA ionic elastomer films, the solution of ionic elastomer was drop casted onto glass slides and cured at room temperature for 12 hours to obtain sample sheets (15 × 4 × 0.08 mm^3). The mechanical testing was performed by a ZwickRoell zwickiLine Z0.5 instrument. All the tensile experiments were performed at room temperature (25°C) with a strain rate of 20 mm/min for both stretching and relaxing steps. The scanning electron microscopy (SEM) images were taken by an FEI Quanta 650 SEM.

To characterize the capacitance of the EDL, ionic elastomer films were prepared with the dimension of 20 × 30 × 0.15 mm^3. Then, the films were sandwiched between two Ag nanoparticle paste electrodes, with an area of 10 × 10 mm^2. The capacitance was measured with a Keysight E4980AL inductance capacitance and resistance (LCR) meter. For the testing of sheet resistance strain of electrodes, electrodes were stretched to varied strains with a customized stretcher, and the resistance values were measured with a customized four-probe platform. To characterize the robustness of electrodes, an electrode was stretched to 50 for 500 times, during which the resistances were measured with the electrometer. The microscope images of ionic elastomer and electrodes were taken with a ZEISS microscope (Axioscope 5).

Sensor characterizations

All the capacitance responses were measured using the LCR meter (at a frequency of 1 kHz and oscillator voltage level of 1 V without dc bias). Pressures were applied by loading varied weights onto the sensors. Cyclic stretching tests of the sensor were done by stretching the sensor to 50% strain for 500 times; the capacitance responses were measured at the 1st, 250th, and 500th cycles, with a pressure of 4 kPa. Cyclic compression tests of the sensor were done by compressing the sensor 500 times with a cyclic pressure of 0.67 kPa under 0 and 50% strains; the capacitance response was recorded throughout the testing by a customized LabVIEW program connected to the LCR meter. The response time was measured by quickly loading 1-kPa pressure on the sensor. To investigate the limit of detection of the sensor, a small piece of paper (0.2 Pa) was repeatedly loaded onto the sensor and the capacitance response was recorded.

E-skin and soft robotic applications

A pneumatically actuated soft robotic hand was integrated with a motorized robotic arm. A conventional stretchable pressure sensor was fabricated without spacers and stiffening microelectrodes. The capacitance of the sensor, which was attached to the fingertip, was measured by an LCR meter in real time and then was transmitted to the control circuit (Arduino) of the robotic arm through the LabVIEW program of the LCR meter. The movement of the

robotic arm is determined by the difference of targeted and current capacitance.

SUPPLEMENTARY MATERIALS

Supplementary material for this article is available at https://science.org/doi/10.1126/sciadv.abi4563

View/request a protocol for this paper from *Bio-protocol*.

REFERENCES AND NOTES

1. M. Sugiyama, T. Uemura, M. Kondo, M. Akiyama, N. Namba, S. Yoshimoto, Y. Noda, T. Araki, T. Sekitani, An ultraflexible organic differential amplifier for recording electrocardiograms. *Nat. Electron.* **2**, 351–360 (2019).
2. T. Araki, T. Uemura, S. Yoshimoto, A. Takemoto, Y. Noda, S. Izumi, T. Sekitani, Wireless monitoring using a stretchable and transparent sensor sheet containing metal nanowires. *Adv. Mater.* **32**, 1902684 (2020).
3. R. Hinchet, H.-J. Yoon, H. Ryu, M.-K. Kim, E.-K. Choi, D.-S. Kim, S.-W. Kim, Transcutaneous ultrasound energy harvesting using capacitive triboelectric technology. *Science* **365**, 491–494 (2019).
4. S. Lee, A. Reuveny, J. Reeder, S. Lee, H. Jin, Q. Liu, T. Yokota, T. Sekitani, T. Isoyama, Y. Abe, Z. Suo, T. Someya, A transparent bending-insensitive pressure sensor. *Nat. Nanotechnol.* **11**, 472–478 (2016).
5. D.-H. Kim, D. C. Kim, Stretchable electronics on another level. *Nat. Electron.* **1**, 440–441 (2018).
6. W. Wang, S. Wang, R. Rastak, Y. Ochiai, S. Niu, Y. Jiang, P. K. Arunachala, Y. Zheng, J. Xu, N. Matsuhisa, X. Yan, S.-K. Kwon, M. Miyakawa, Z. Zhang, R. Ning, A. M. Foudeh, Y. Yun, C. Linder, J. B.-H. Tok, Z. Bao, Strain-insensitive intrinsically stretchable transistors and circuits. *Nat. Electron.* **4**, 143–150 (2021).
7. S. Han, J. Kim, S. M. Won, Y. Ma, D. Kang, Z. Xie, K.-T. Lee, H. U. Chung, A. Banks, S. Min, S. Y. Heo, C. R. Davies, J. W. Lee, C.-H. Lee, B. H. Kim, K. Li, Y. Zhou, C. Wei, X. Feng, Y. Huang, J. A. Rogers, Battery-free, wireless sensors for full-body pressure and temperature mapping. *Sci. Transl. Med.* **10**, eaan4950 (2018).
8. S. Choi, S. I. Han, D. Jung, H. J. Hwang, C. Lim, S. Bae, O. K. Park, C. M. Tschabrunn, M. Lee, S. Y. Bae, J. W. Yu, J. H. Ryu, S.-W. Lee, K. Park, P. M. Kang, W. B. Lee, R. Nezafat, T. Hyeon, D.-H. Kim, Highly conductive, stretchable and biocompatible Ag–Au core–sheath nanowire composite for wearable and implantable bioelectronics. *Nat. Nanotechnol.* **13**, 1048–1056 (2018).
9. C. M. Boutry, L. Beker, Y. Kaizawa, C. Vassos, H. Tran, A. C. Hinckley, R. Pfattner, S. Niu, J. Li, J. Claverie, Z. Wang, J. Chang, P. M. Fox, Z. Bao, Biodegradable and flexible arterial-pulse sensor for the wireless monitoring of blood flow. *Nat. Biomed. Eng.* **3**, 47–57 (2019).
10. Y. Dai, H. Hu, M. Wang, J. Xu, S. Wang, Stretchable transistors and functional circuits for human-integrated electronics. *Nat. Electron.* **4**, 17–29 (2021).
11. C. Larson, B. Peele, S. Li, S. Robinson, M. Totaro, L. Beccai, B. Mazzolai, R. Shepherd, Highly stretchable electroluminescent skin for optical signaling and tactile sensing. *Science* **351**, 1071–1074 (2016).
12. S. Wang, J. Xu, W. Wang, G.-J. N. Wang, R. Rastak, F. Molina-Lopez, J. W. Chung, S. Niu, V. R. Feig, J. Lopez, T. Lei, S.-K. Kwon, Y. Kim, A. M. Foudeh, A. Ehrlich, A. Gasperini, Y. Yun, B. Murmann, J. B.-H. Tok, Z. Bao, Skin electronics from scalable fabrication of an intrinsically stretchable transistor array. *Nature* **555**, 83–88 (2018).
13. S. Sankar, D. Balamurugan, A. Brown, K. Ding, X. Xu, J. H. Low, C. H. Yeow, N. Thakor, Texture discrimination with a soft biomimetic finger using a flexible neuromorphic tactile sensor array that provides sensory feedback. *Soft Robot.* **8**, 577–587 (2021).
14. F. A. Hassani, H. Jin, T. Yokota, T. Someya, N. V. Thakor, Soft sensors for a sensing-actuation system with high bladder voiding efficiency. *Sci. Adv.* **6**, eaba0412 (2020).
15. H. Bai, S. Li, J. Barreiros, Y. Tu, C. R. Pollock, R. F. Shepherd, Stretchable distributed fiber-optic sensors. *Science* **370**, 848–852 (2020).
16. K. W. O'Brien, P. A. Xu, D. J. Levine, C. A. Aubin, H.-J. Yang, M. F. Xiao, L. W. Wiesner, R. F. Shepherd, Elastomeric passive transmission for autonomous force-velocity adaptation applied to 3D-printed prosthetics. *Sci. Robot.* **3**, eaau5543 (2018).
17. M. Wang, Z. Yan, T. Wang, P. Cai, S. Gao, Y. Zeng, C. Wan, H. Wang, L. Pan, J. Yu, S. Pan, K. He, J. Lu, X. Chen, Gesture recognition using a bioinspired learning architecture that integrates visual data with somatosensory data from stretchable sensors. *Nat. Electron.* **3**, 563–570 (2020).
18. S. Niu, N. Matsuhisa, L. Beker, J. Li, S. Wang, J. Wang, Y. Jiang, X. Yan, Y. Yun, W. Burnett, A. S. Y. Poon, J. B.-H. Tok, X. Chen, Z. Bao, A wireless body area sensor network based on stretchable passive tags. *Nat. Electron.* **2**, 361–368 (2019).
19. L. Pan, F. Wang, Y. Cheng, W. R. Leow, Y.-W. Zhang, M. Wang, P. Cai, B. Ji, D. Li, X. Chen, A supertough electro-tendon based on spider silk composites. *Nat. Commun.* **11**, 1332 (2020).
20. Q. Hua, J. Sun, H. Liu, R. Bao, R. Yu, J. Zhai, C. Pan, Z. L. Wang, Skin-inspired highly stretchable and conformable matrix networks for multifunctional sensing. *Nat. Commun.* **9**, 244 (2018).
21. F. Zhang, Y. Zang, D. Huang, C. Di, D. Zhu, Flexible and self-powered temperature–pressure dual-parameter sensors using microstructure-frame-supported organic thermoelectric materials. *Nat. Commun.* **6**, 8356 (2015).
22. B. W. An, S. Heo, S. Ji, F. Bien, J.-U. Park, Transparent and flexible fingerprint sensor array with multiplexed detection of tactile pressure and skin temperature. *Nat. Commun.* **9**, 2458 (2018).
23. S. Lee, S. Franklin, F. A. Hassani, T. Yokota, O. G. Nayeem, Y. Wang, R. Leib, G. Cheng, D. W. Franklin, T. Someya, Nanomesh pressure sensor for monitoring finger manipulation without sensory interference. *Science* **370**, 966–970 (2020).
24. Y. Zhang, S. Liu, Y. Miao, H. Yang, X. Chen, X. Xiao, Z. Jiang, X. Chen, B. Nie, J. Liu, Highly stretchable and sensitive pressure sensor array based on icicle-shaped liquid metal film electrodes. *ACS Appl. Mater. Interfaces* **12**, 27961–27970 (2020).
25. C.-L. Choong, M.-B. Shim, B.-S. Lee, S. Jeon, D.-S. Ko, T.-H. Kang, J. Bae, S. H. Lee, K.-E. Byun, J. Im, Y. J. Jeong, C. E. Park, J.-J. Park, U.-I. Chung, Highly stretchable resistive pressure sensors using a conductive elastomeric composite on a micropyramid array. *Adv. Mater.* **26**, 3451–3458 (2014).
26. E. Roh, H.-B. Lee, D.-I. Kim, N.-E. Lee, A solution-processable, omnidirectionally stretchable, and high-pressure-sensitive piezoresistive device. *Adv. Mater.* **29**, 1703004 (2017).
27. J. C. Yang, J.-O. Kim, J. Oh, S. Y. Kwon, J. Y. Sim, D. W. Kim, H. B. Choi, S. Park, Microstructured porous pyramid-based ultrahigh sensitive pressure sensor insensitive to strain and temperature. *ACS Appl. Mater. Interfaces* **11**, 19472–19480 (2019).
28. Y. Cheng, R. Wang, H. Zhai, J. Sun, Stretchable electronic skin based on silver nanowire composite fiber electrodes for sensing pressure, proximity, and multidirectional strain. *Nanoscale* **9**, 3834–3842 (2017).
29. B.-U. Hwang, A. Zabeeb, T. Q. Trung, L. Wen, J. D. Lee, Y.-I. Choi, H.-B. Lee, J. H. Kim, J. G. Han, N.-E. Lee, A transparent stretchable sensor for distinguishable detection of touch and pressure by capacitive and piezoresistive signal transduction. *NPG Asia Mater.* **11**, 23 (2019).
30. H. Qin, R. E. Owyeung, S. R. Sonkusale, M. J. Panzer, Highly stretchable and nonvolatile gelatin-supported deep eutectic solvent gel electrolyte-based ionic skins for strain and pressure sensing. *J. Mater. Chem. C* **7**, 601–608 (2019).
31. C. M. Boutry, Y. Kaizawa, B. C. Schroeder, A. Chortos, A. Legrand, Z. Wang, J. Chang, P. Fox, Z. Bao, A stretchable and biodegradable strain and pressure sensor for orthopaedic application. *Nat. Electron.* **1**, 314–321 (2018).
32. R. Sarkar, T. K. Kundu, Nonbonding interaction analyses on PVDF/[BMIM][BF4] complex system in gas and solution phase. *J. Mol. Model.* **25**, 131 (2019).
33. X. Wang, C. Yang, G. Wang, Stretchable fluoroelastomer quasi-solid-state organic electrolyte for high-performance asymmetric flexible supercapacitors. *J. Mater. Chem. A* **4**, 14839–14848 (2016).
34. C. Pang, G.-Y. Lee, T. Kim, S. M. Kim, H. N. Kim, S.-H. Ahn, K.-Y. Suh, A flexible and highly sensitive strain-gauge sensor using reversible interlocking of nanofibres. *Nat. Mater.* **11**, 795–801 (2012).

Acknowledgments

Funding: This work was funded by Start-up fund from the University of Chicago, the U.S. Office of Naval Research Young Investigator award N00014-21-1-2581, and National Science Foundation award DMR-2011854. J.X. acknowledges the Center for Nanoscale Materials, a U.S. Department of Energy Office of Science User Facility, and supported by the U.S. Department of Energy, Office of Science, under contract no. DE-AC02-06CH11357. **Author contributions:** Q.S. and S.W. designed the project and experiments. Q.S. fabricated the stretchable and strain-unperturbed pressure sensors and carried out electrical and mechanical characterizations. Ya.L fabricated the silicon mold. Y.C. and L.J. carried out mechanical simulations. S.-Y.T., R.N., A.M., and P.L. programmed the closed-loop control of pressure. N.L. carried out Fourier transform infrared spectroscopy characterizations. W.L. carried out thermogravimetric characterizations. P.C., S.D., and Yo.L helps with sensor fabrication and measurements. Q.S., S.W., and J.T.K. wrote the manuscript. All authors reviewed and commented on the manuscript. **Competing interests:** S.W., Q.S., and Ya.L are inventors on a pending patent filed by The University of Chicago (no. 63/193,819, filed 27 May 2021). The authors declare that they have no other competing interests. **Data and materials availability:** All data needed to evaluate the conclusions in the paper are present in the paper and/or the Supplementary Materials.

Submitted 10 March 2021
Accepted 5 October 2021
Published 24 November 2021
10.1126/sciadv.abi4563